Journal of Computational Physics **156,** 360–381 (1999)
Article ID jcph.1999.6375, available online at http://www.idealibrary.com on IDEAL®

A Spectral-Element Method for Particulate Stokes Flow

C. Pozrikidis

University of California, San Diego, La Jolla, California 92093-0411
E-mail: cpozrikidis@ucsd.edu

Received January 21, 1999; revised September 10, 1999

A numerical procedure is presented for solving the equations of Stokes flow past a fixed bed of rigid particles and the equations describing the motion of a suspension of rigid particles upon which a specified force and torque is exerted, for general flow configurations and arbitrary particle shapes. The problem is formulated in terms of an integral equation of the first kind for the distribution of the boundary traction incorporating a Green function that observes the periodicity of the flow and the geometry of the boundaries of the flow, accompanied by appropriate boundary conditions and integral constraints. The integral equation is solved for two-dimensional flow by a spectral-element orthogonal-collocation method. Two important components of the numerical method are (a) preconditioning of the linear system that arises from the discretization of integral equation followed by reduction to remove the eigenfunctions corresponding to the null eigenvalue over each particle surface and (b) a physically motivated iterative solution of the master linear system based on particle clustering. It is found that, for the purpose of computing the force and torque exerted on fixed particles and the velocity of translation and angular velocity of rotation of freely suspended particles, the orthogonal collocation method has significant advantages over the trapezoidal discretization. The iterative solution of the integral equation converges even for closely spaced particles where each particle is treated as a cluster. © 1999 Academic Press

Key Words: boundary-integral methods; boundary-element methods; spectral-element methods; particulate flow; Stokes flow.

I. INTRODUCTION

Viscous flows past fixed beds of particles and flows of suspensions of rigid particles arise in a broad spectrum of natural, physiological, and engineering applications. The diversity of these flows is best demonstrated by citing a few characteristic examples.

Flow past fixed beds of particles has been studied with reference to the hydrodynamics of consolidated and non-consolidated porous media. Investigations of flow through regular

0021-9991/99 $30.00
Copyright © 1999 by Academic Press
All rights of reproduction in any form reserved.

and random arrays yield information on the dependencies of the medium permeability and species dispersivity on the geometry of the microstructure. Flow through fibrous matrices consisting of networks of slender particles is encountered in the fabrication of absorbent tissues and industrial composites, and their modeling provides guidelines for the engineering design of these materials. Suspensions of rigid particles occur in a large number of industrial processes, such as slurry transport, photographic emulsion coating, paste manufacturing, and foodstuff handling. The study of the rheological and transport properties of these suspensions and the analysis of the dynamics of their microstructure define an important field of fundamental and applied research. Finally, two-dimensional suspensions of cylindrical particles have been studied as models of bilayered biological membranes hosting proteins. Among other properties, the protein diffusivity may be estimated by dynamical simulation using methods of hydrodynamics.

In the vast majority of the aforementioned applications, the size of the particles is small, the flow occurs at effectively zero Reynolds number, and the motion may be described on the basis of the linearized equations of Stokes flow. Early investigations of viscous particulate flows considered configurations with one or two interacting particles using analytical, semi-analytical, and perturbations methods. Reviews were given by Happel and Brenner [1] and, more recently, by Kim and Karrila [2]. The development of efficient and accurate numerical methods that allow the simulation of systems containing a large number of particles with arbitrary shapes has been a long-standing desire. Over the past 15 years, theoretical advances in the field of computational particulate microhydrodynamics and the availability of computing power have allowed the development of several viable approaches, as will be reviewed in the remainder of this Introduction. In this discussion, we do not include methods for flows with suspended deformable particles including drops, bubbles, and capsules [e.g., 3]. An overview of methods for simulating these flows will be given in a forthcoming special issue of this journal dedicated to multi-phase flow [4].

Early efforts to perform large-scale numerical simulations of suspensions of rigid particles are reviewed by Barnes *et al*. [5]. The development of the Stokesian dynamics method by Brady and co-workers and others considerably enhanced our ability to simulate large-size systems [6–8]. The numerical algorithm combines the method of multi-pole expansions originating from the boundary-integral representation to account for far-field interaction, Faxen's laws to compute the force and torque exerted on a particle due to the flow induced by all other particles, and lubrication-flow corrections to account for near-contact interactions. The method has been used on several occasions to simulate flows past fixed arrays of spherical particles and flows of monodisperse and polydisperse suspensions of spherical particles (e.g., [9–11]). A generalization of the method to account for non-spherical particles shapes is possible [12], but the loss of numerical efficiency and analyticaly tractability is a practical impediment.

Sangani and Mo [13] developed an improved version of the method of Stokesian dynamics, whose distinguishing feature is that lubrication forces developing between neighboring spherical or circular particles are modeled by point-force-dipole singularities placed at the gaps. In a subsequent study [14], the improved method was combined with a fast summation algorithm that is able to handle sums over a large number of Stokes flow singularities resulting from the multi-pole expansions. The integrated approach yields a powerful algorithm that can be used to simulate systems of large size. An extension of the method to non-spherical or non-circular shapes has not been developed.

In addition to the preceding approaches, lattice Boltzmann methods for viscous flows were developed by Ladd (e.g., [15]), and finite-element methods were developed by Hu [16]. The former allows the simulation of a large number of particles, on the order of several thousand, and is able to handle flows at vanishing as well as non-zero Reynolds numbers. On the downside, the accuracy of the method has not been discussed in detail, and the implementation involves specialized algorithms that lie beyond the main stream of fluid dynamics. The finite-element method combines an impressive collection of algorithms for dynamic regridding, but demands substantial computational resources.

The ability to compute Stokes flow by solving an integral equation of the first kind for the distribution of the traction over a particle surface was first demonstrated by Youngren and Acrivos [17]. Although the method has been applied widely to study a variety of internal and external flows, only a limited number of numerical simulations of multi-particle systems have been carried out (e.g., [18–20]). A serious concern is the non-uniqueness of solution of the integral equation resulting in nearly singular linear systems whose condition number increases rapidly as the numerical error becomes smaller (e.g., [21, p. 207]). Although, in practice, ill-conditioning may not be detrimental for the accuracy of the solution, it nevertheless casts a shadow of doubt on the reliability of the numerical method. Practical concerns associated with high computational times required for compiling the influence matrix and then solving the dense linear system resulting from the discretization of the integral equation also arise. These concerns, however, are typical of generalized multi-particle systems and may be addressed with the implementation of general-purpose methods [14].

To circumvent the issue of non-uniqueness of the integral equation, Power and Miranda [22] and Kim and Karrila [2] developed a completed double-layer representation that formulates the problem in terms of an integral equation of the second kind with a unique solution for the fictitious density of a double-layer potential (see also [23, Chap. 4]). In the case of the mobility problem, where the force and torque exerted on the particles are specified and the translational and angular velocities are to be computed, the deflated integral equation may be solved by the method of successive substitutions, and the translational and angular velocities arise as part of the solution. Phan-Thien and Kim [21, pp. 228–229] present results of a numerical simulation of the motion of 1320 particles carried out on a network of 11 workstations with parallel processing using the PVM communications protocol.

In a complementary approach, Kim and Karrila [2] and Fan *et al*. [24] formulated the mobility problem in terms of an integral equation of the second kind with a unique solution for the distribution of the traction over the particle surfaces. The weakly singular kernel of the integral operator is the adjoint of that of the double-layer potential. A more general formulation that incorporates a hypersingular integral in the forcing term of the integral equation was discussed by Ingber and Mondy [25]. Fan *et al*. [24] presented numerical solutions for the instantaneous flow of triply periodic suspensions with up to 33 particles, conducted on parallel processors. To this end, we point out that in most applications of particulate flow, the quantities of primary interest are the force and torque exerted on a stationary particle or the velocity and rate of rotation of a moving particle. The traction distribution or density of a fictitious hydrodynamic potential is significant only insofar as it is able to produce these macroscopic variables, and their computation may be regarded as an inevitable intermediate step.

In this work, we develop and study several aspects of the direct boundary-integral method for Stokes flow past rigid particles, formulated in terms of an integral equation of the first

kind for the distribution of the traction over the particle surfaces and involving the single-layer hydrodynamic potential. Advantages of the single-layer formulation compared to the double-layer formulation and its adjoint are conceptual simplicity, resulting in computer memory savings, and economical evaluation of the Green's function kernels. First, we implement a spectral-element orthogonal-collocation method for solving the integral equation of the first kind and assess its efficiency in comparison with the trapezoidal discretization. Similar collocation methods for solving integral equations of two- and three-dimensional Stokes flow were developed by Occhialini *et al*. [26] and Muldowney and Higdon [27]. Here, we focus on the aspects of the method pertaining to particulate flow. Second, we develop a method for eliminating the multiplicity of solutions of the integral equation by projecting the linear system that arises from the single-layer discretization into the space that is orthogonal to the discretized eigenvectors of the transpose of the single-layer potential. Third, we show that a simple iterative procedure for solving the linear system based on particle clustering converges even in the case of closely spaced particles.

In Sections II and III, we introduce two related boundary-integral formulations and associated numerical methods. The first formulation pertains to the resistance problem involving viscous flow past a fixed bed of rigid particles, and the second formulation pertains to the mobility problem involving the flow of a suspension of rigid particles upon which a specified force and torque are exerted. The formulations are developed with reference to two-dimensional flow, but this is done only to facilitate the presentation and to allow us to perform extensive numerical experimentation. Analogous formulations for three-dimensional flow arise by straightforward, albeit nontrivial generalizations, as will be discussed in the concluding section.

II. FLOW PAST A FIXED BED OF PARTICLES

Consider Stokes flow past a fixed bed of two-dimensional particles, as depicted in Fig. 1. To develop the boundary-integral formulation, we decompose the velocity field into the unperturbed component denoted as $\boldsymbol{u}^\infty$ and a disturbance component denoted as $\boldsymbol{u}^{\mathrm{D}}$. The incident velocity is defined as follows:

- For shear flow past a solitary or periodic collection of particles above a plane wall located at $y = w$, as illustrated in Figs. 1a, 1b,

$$u_x^\infty = k(y - w) + \frac{1}{2}\frac{\delta}{\mu}(y - w)^2, \quad u_y^\infty = 0, \tag{1}$$

where k is the shear rate at the wall, δ is the pressure gradient, and μ is the fluid viscosity. The associated incident pressure field is given by $p^\infty = \delta x$. In Fig. 1b, L is the period of the flow.

- For flow past a periodic collection of particles in a channel that is confined between two parallel plane walls, as illustrated in Fig. 1c,

$$u_x^\infty = U_1 + (U_2 - U_1)\frac{y + h}{2h} + \frac{1}{2}\frac{\delta}{\mu}(y^2 - h^2), \quad u_y^\infty = 0. \tag{2}$$

The channel centerline is located at $y = 0$, h is the channel semi-width, U_1 is the velocity of the lower wall, U_2 is the velocity of the upper wall, and δ is the pressure gradient. The associated incident pressure field is given by $p^\infty = \delta x$.

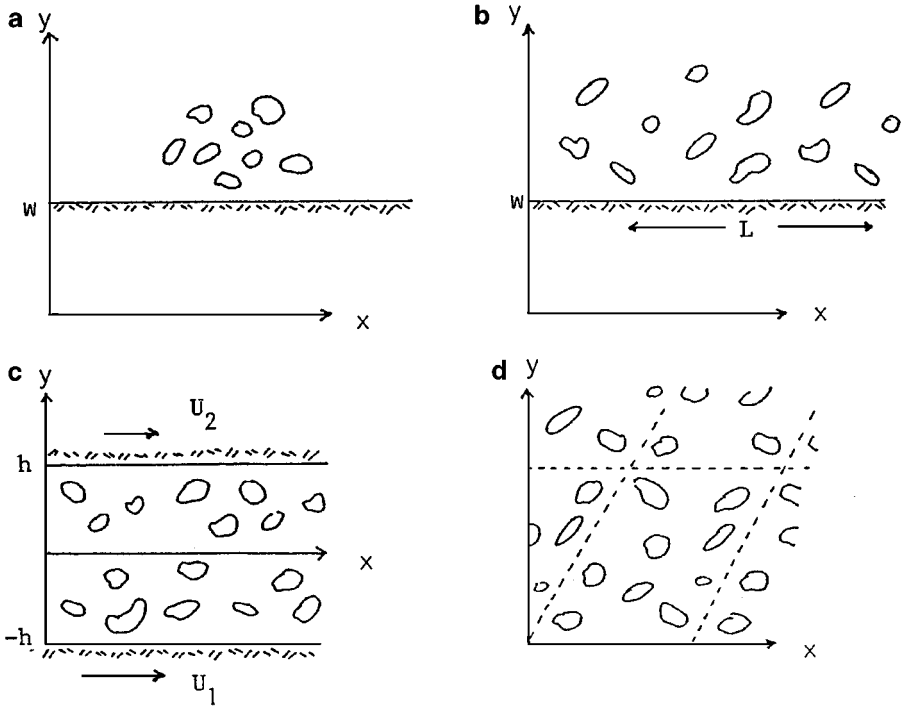

FIG. 1. Schematic illustration of several configurations involving flow past a fixed bed of rigid particles or flow of a suspension of rigid particles upon which a specified force and torque is exerted.

• For uniform flow past a doubly periodic array of particles representing, for example, a porous medium, as illustrated in Fig. 1d,

$$u_x^\infty = U, \quad u_y^\infty = 0, \tag{3}$$

where U is the constant velocity of the incident flow determining the flow rate through the array. The associated pressure field is uniform.

To avoid the ill-posedness of two-dimensional Stokes flow in a unbounded domain, we consider shear flow, doubly periodic flow, and flow bounded by an infinite wall. The distribution of the traction over the particle surfaces, $\boldsymbol{f} = \boldsymbol{\sigma} \cdot \boldsymbol{n}$, where $\boldsymbol{\sigma}$ is the Newtonian stress tensor and $\boldsymbol{n}$ is the unit vector normal to the particle contours pointing into the fluid, satisfies the integral equation of the first kind

$$\int_C G_{ji}(\boldsymbol{x}_0, \boldsymbol{x})\, f_i(\boldsymbol{x})\, dl(\boldsymbol{x}) = 4\pi\mu\, u_j^\infty(\boldsymbol{x}_0), \tag{4}$$

where C is the collection of all particle contours, the point $\boldsymbol{x}_0$ lies on C, l is the arc length along C, and $\boldsymbol{G}$ is the Green's function of the equations of Stokes flow observing the periodicity and respecting the geometry of the boundaries of the flow under consideration [22]. The Green's functions for all types of flows illustrated in Fig. 1 are available in closed or transcendental but readily computable form (e.g., [23, 28]). It is important to emphasize that all information regarding the flow periodicity or boundary geometry is carried by the

Green's function, and an explicit consideration of the boundaries is not required. Thus, the numerical methods to be discussed are applicable to a broad range of flows selected by an appropriate choice for the Green's function.

The Green's functions of Stokes flow satisfy the symmetry property

$$G_{ji}(\boldsymbol{x}_0, \boldsymbol{x}) = G_{ij}(\boldsymbol{x}, \boldsymbol{x}_0), \tag{5}$$

which ensures that the integral operator on the left-hand side of (4) is self-adjoint.

The integral equation (4) has an infinite number of solutions: conservation of mass for the flow induced by a point force requires that

$$\int_{C_k} n_j(\boldsymbol{x}_0)\, G_{ji}(\boldsymbol{x}_0, \boldsymbol{x})\, dl(\boldsymbol{x}_0) = 0, \tag{6}$$

where C_k is the contour of the kth particle. Combining this identity with the symmetry property (5), we find

$$\int_{C_k} G_{ji}(\boldsymbol{x}_0, \boldsymbol{x}) n_i(\boldsymbol{x})\, dl(\boldsymbol{x}) = 0. \tag{7}$$

Because of identity (7), any particular solution of the integral equation (4) over a particle surface may be enhanced with an arbitrary multiple of the normal vector. To this end, it should be pointed out that the density of the single-layer potential in (4) is a generalized mathematical traction playing the role of a distribution density. The physical traction arises by using the boundary-integral representation to evaluate the stress in terms of the corresponding Green's function.

Projecting both sides of (4) onto the normal vector on the kth particle, integrating with respect to arc length around the particle contour, and using identity (6), we obtain the solvability condition for (4)

$$\int_{C_k} R_i(\boldsymbol{x})\, n_i(\boldsymbol{x})\, dl(\boldsymbol{x}) = 0, \tag{8}$$

where $\boldsymbol{R}$ stand for the right-hand side of (4). Fortunately, this condition is satisfied for any incompressible incident flow, including the flows described by Eqs. (1)–(3).

A. *Orthogonal Collocation*

In practice, Eq. (4) is solved routinely by boundary-element methods. First, each particle contour is discretized into a collection of elements that may be straight segments, parabolic or high-order elements, or native elements of the particle shapes considered. Second, the traction over each element is approximated with a truncated expansion of basis functions of a selected class. In the simplest approach, the traction over each element is assumed to be constant, corresponding to the trapezoidal discretization. Requiring the satisfaction of the integral equation (4) at an appropriate number of collocation points, we obtain a linear system of equations for the coefficients of the basis functions. For the purpose of computing integrals of the traction and its moments with respect to arc length, the trapezoidal discretization might appear to be the best choice: the Euler–MacLaurin formula appears to indicate that these integrals converge at a super-algebraic rate. The singular nature of

the Green's function, however, introduces algebraic error terms that decelerate the rate of convergence.

We implemented an orthogonal collocation method with polynomial basis functions over each boundary element along the particle contours for solving the integral equation (4). The Cartesian components of the traction are expressed in terms of an expansion of $m+1$ polynomials over each element, where m is the highest polynomial order. The independent variable of the local expansion is the scaled native parameter that describes the shape of the boundary element, varying over the interval $[-1, 1]$ from the first to the second end point. The $m+1$ collocation points are placed at the scaled zeros of an $(m+1)$-degree orthogonal polynomial of a certain class. The simplest choice, $m=0$, approximates the traction with a constant function over each element and requires one collocation point. Following the standard implementation of the spectral-element method in terms of nodal expansions [e.g., 29], we express the polynomial expansion over each element in terms of Lagrange interpolation polynomials multiplied by the values of the traction at the collocation points. The influence matrix of the integral equation is computed numerically by the method of impulses, which involves (a) setting the value of the traction at all collocation points equal to zero except at one test point where one component is set equal to unity and (b) computing numerically the single-layer integral on the left-hand side of (4) at all collocation points.

The Green's function exhibits a logarithmic singularity at the collocation points that share an element with the test point. The corresponding Lagrange polynomials take the value of unity at the test point and vanish, at a generally linear rate, at all other element collocation points termed the non-singular native collocation points. Consequently, the integrand of the single-layer potential is singular at the test point and regular at the non-singular native collocation points. Since, however, the derivatives of the integrand are singular at the non-singular native collocation points, the use of the Gauss–Legendre quadrature to compute the weakly singular boundary integrals introduces a substantial amount of numerical error that causes the solution of the linear system to be visibly sensitive to the number of Gauss–Legendre integration points employed. Numerical experimentation showed that even 20 Gauss–Legendre quadrature points over each element are not sufficient for obtaining a solution that is independent of the number of quadrature points.

To circumvent this difficulty, we subtract the product of the logarithmic singularity and the Lagrange interpolation polynomials from the single-layer potential and then compute it with high accuracy using a four- or five-point integration quadrature for integrands with a logarithmic singularity. The integration is performed with respect to the natural parameter of the boundary-element shape. The five-point quadrature integrates exactly integrals with Lagrange interpolants of degree less than or equal to 9, which is sufficient for the purposes of the present study. The remaining regular integrals are computed by the 6- or 12-point Gauss–Legendre quadrature. With this implementation, the results are confirmed to be independent of the number of quadrature points at least up to the eighth significant figure.

In the majority of applications, we are interested in the force and torque exerted on the particles for the purpose of estimating, for example, the permeability of a porous medium or the resistivity of a membrane. This practical desire motivates placing the collocation points at scaled zeros of Legendre polynomials so that, in the absence of singularities, the integral of the traction with respect to arc length can be computed directly from the numerical solution with the highest possible accuracy using the Gauss–Legendre quadrature. Accordingly, the collocation points were placed at the scaled zeros of Legendre polynomials over the boundary elements.

After the integral equation has been discretized and applied at the collocation point, we obtain a linear algebraic system for the Cartesian components of the traction at the collocation points,

$$\boldsymbol{A}\,\boldsymbol{z} = \boldsymbol{b}, \tag{9}$$

where $\boldsymbol{A}$ is the master influence matrix and $\boldsymbol{b}$ is a constant vector. The size of the system (9) is equal to twice the number of boundary elements over all particles. The vector $\boldsymbol{z}$ contains the unknown x and y components of the traction at the collocation points over all elements, arranged in the lexicographic order

$$\begin{aligned}\boldsymbol{z} = \big(&f_x^{1,1},\ f_x^{1,2},\ldots,\ f_x^{1,N_{c,1}},\ f_y^{1,1},\ f_y^{1,2},\ldots,\ f_y^{1,N_{c,1}}\\ &,f_x^{2,1},\ f_x^{2,2},\ldots,\ f_x^{2,N_{c,2}},\ f_y^{2,1},\ f_y^{2,2},\ldots,\ f_y^{2,N_{c,2}}\\ &\ldots\\ &,f_x^{i,1},\ f_x^{i,2},\ldots,\ f_x^{i,N_{c,i}},\ f_y^{i,1},\ f_y^{i,2},\ldots,\ f_y^{i,N_{c,i}}\\ &\ldots\\ &,f_x^{N,1},\ f_x^{N,2},\ldots,\ f_x^{N,N_{c,N}},\ f_y^{N,1},\ f_y^{N,2},\ldots,\ f_y^{N,N_{c,N}}\big),\end{aligned} \tag{10}$$

where $f_x^{i,j}$ is the x component of the traction on the jth element of the ith particle, $N_{c,i}$ is the number of collocation points around the contour of the ith particle, and N is the number of particles; $f_y^{i,j}$ is defined in a similar way. The individual scalar equations in system (9) are arranged in an order corresponding to (10).

B. *Preconditioning*

The discrete form of the integral identity (7) corresponding to the discretization underlying the linear system (9) is

$$\boldsymbol{A}\,\boldsymbol{w}^{(k)} = 0, \tag{11}$$

$k = 1, \ldots, N$, where the discrete exact or approximate eigenvector $\boldsymbol{w}^{(k)}$ contains the x and y components of the normal vector at the collocation points around the kth particle contour. When the boundary elements are straight segments, in which case the discretized particle contour is polygonal, the normal vector over each element is constant, and condition (11) is satisfied up to the numerical error associated with the numerical computation of the elements of the master influence matrix. In the present implementation where highly accurate numerical integration is employed, the numerical error is comparable to the round-off error. More generally, as the discretization error is reduced by increasing the number of collocation points, $\boldsymbol{w}^{(k)}$ reduces to an exact eigenvector.

The discussion in the previous paragraph suggests that the matrix $\boldsymbol{A}$ introduced in Eq. (9) is nearly or precisely singular, reflecting the non-uniqueness of solution of the integral equations (4); as the truncation error is reduced, the condition number is raised (e.g., [21, p. 207]). To the author's knowledge, in all previous numerical solutions of this or similar integral equations, the nearly singular behavior of the master linear matrix was ignored, and the numerical method had to rely on the discretization error, the

round-off error, or the inherent geometrical symmetry of the flow to produced a sensible solution. General methods for regularizing nearly singular algebraic systems by spectrum deflation have been discussed by several authors (e.g., [30–32]). In the present case, knowledge of the adjoint eigenvectors of the single-layer potential corresponding to the null eigenvalue allows us to perform preconditioning with the least amount of perturbation.

The discrete form of the right-hand side of the solvability condition (8) corresponding to the discretization underlying the system (9) is

$$\sum_j \big(R_i^{(k)}\big)_j \big(n_i^{(k)}\big)_j h_j^{(k)}, \tag{12}$$

where j runs over the collocation points around the contour of the kth particle, and $h_j^{(k)}$ is an integration weight with respect to arc length associated with the Gauss–Legendre quadrature, playing the role of a discrete metric. When the particle contour is polygonal and the vector $\boldsymbol{R}$ varies in a polynomial-like manner over an element with a degree that is lower than that required for exact integration by use of the Gauss–Legendre quadrature, subject to the available number of collocation points, the discrete form of the solvability condition is satisfied to machine accuracy.

To render the system (9) singular while guaranteeing an infinity of solutions, we premultiply both sides of it by the preconditioning matrix $\boldsymbol{P}$ defined as

$$\boldsymbol{P} = \prod_{k=1}^{N} \big(\boldsymbol{I} - \boldsymbol{v}^{(k)^{\mathrm{T}}} \boldsymbol{v}^{(k)}\big), \tag{13}$$

where the superscript T stands for the transpose, and the vectors $\boldsymbol{v}^{(k)}$ are global adjoint eigenvectors with the following properties: the length of $\boldsymbol{v}^{(k)}$ is equal to twice the total number of collocation points over all particles; all components of $\boldsymbol{v}^{(k)}$ are equal to zero except for the components corresponding to the kth particle block on the right-hand side of (10) that hosts the local discrete eigenvector $\alpha^{(k)}(n_i^{(k)})_j h_j^{(k)}$, $j = 1, \ldots, N_{\mathrm{c},i}$, where summation is not implied over j, and $\alpha^{(k)}$ is a scaling coefficient adjusted so that the length of $\boldsymbol{v}^{(k)}$ is equal to unity. Since the set $\boldsymbol{v}^{(k)}$ is orthogonal, the order of multiplication on the right-hand side of (13) is immaterial. In the numerical implementation, only those rows and columns of the matrix $\boldsymbol{A}$ corresponding to the non-zero entries of $\boldsymbol{v}^{(k)}$ are altered during the kth projection.

After preconditioning, the system (9) takes the form

$$\boldsymbol{A}^{\mathrm{P}} \boldsymbol{z}^{\mathrm{P}} = \boldsymbol{b}^{\mathrm{P}}, \tag{14}$$

where $\boldsymbol{A}^{\mathrm{P}} = \boldsymbol{PA}$, $\boldsymbol{b}^{\mathrm{P}} = \boldsymbol{Pb}$, and the superscript P stands for preconditioned. The vector $\boldsymbol{v}^{(k)}$ is an exact eigenvector of the transpose of the singular matrix $\boldsymbol{A}^{\mathrm{P}}$ corresponding to the zero eigenvalue, and the following solvability condition is also satisfied to machine accuracy:

$$\boldsymbol{v}^{(i)} \cdot \boldsymbol{b}^{\mathrm{P}} = \boldsymbol{0}. \tag{15}$$

Thus, the projection guarantees the satisfaction of both the integral identity (6) and the solvability condition (8), while introducing the mildest possible perturbation of the right-hand side: when expression (12) is equal to zero, the projection has no effect on the right-hand side.

C. *Reduction*

To obtain one solution of the singular system (14), we set the value of the y component of the traction at the last collocation point around each particle equal to an arbitrary value that was chosen to be zero, $f_y^{i,N_{c,i}} = 0$, $i = 1, 2, \ldots, N$. This is permissible as long as the corresponding normal vector does not point in the x direction; if it does, then another unknown can be set equal to zero. Discarding the corresponding equations from system (14), we obtain the system

$$\boldsymbol{A}^{\mathrm{PR}}\boldsymbol{z}^{\mathrm{R}} = \boldsymbol{b}^{\mathrm{PR}}, \tag{16}$$

where the superscript R stands for reduced. Equation (16) has a unique solution that may be computed using any dense-system linear solver, for example, a solver based on Gauss elimination.

D. *Iterative Solution*

Even with a moderate number of particles, the computational cost required for solving the linear system is unaffordable. In practical applications, we are interested in flows with at least 25 particles and require a minimum of 32 collocation points around each particle for reasonable accuracy, corresponding to a linear system with 1600 unknowns. It is imperative that the linear system be solved by an iterative method.

We have implemented a physically motivated iterative method that is similar to the domain decomposition method developed by Phan-Thien and Tullock with reference to the adjoint double-layer representation [33]. The idea is to recast the primary or preconditioned and reduced linear system into the form

$$\boldsymbol{M}^{\mathrm{Q}}\boldsymbol{z} = \boldsymbol{N}^{\mathrm{Q}}\boldsymbol{z} + \boldsymbol{b}^{\mathrm{Q}}, \tag{17}$$

where the qualifier Q either is absent or stands for PR, and then perform Jacobi or Gauss–Siedel iterations based on the recursion formula

$$\boldsymbol{M}^{\mathrm{Q}}\boldsymbol{z}^{(k+1)} = \boldsymbol{N}^{\mathrm{Q}}\boldsymbol{z}^{(k)} + \boldsymbol{b}^{\mathrm{D}}, \tag{18}$$

where the superscript (k) designates the number of iterations. The form of (18) is based on the splitting $\boldsymbol{A}^{\mathrm{Q}} = \boldsymbol{M}^{\mathrm{Q}} - \boldsymbol{N}^{\mathrm{Q}}$, where $\boldsymbol{M}^{\mathrm{Q}}$ is a block-diagonal matrix whose blocks correspond to *particle clusters*. The individual equations corresponding to particle clusters have been decoupled, and solving for $\boldsymbol{z}^{(k+1)}$ requires the inversion of diagonal blocks. When only one particle cluster is defined encompassing all particles, $\boldsymbol{M}^{\mathrm{Q}} = \boldsymbol{A}$, $\boldsymbol{N}^{\mathrm{Q}} = \boldsymbol{0}$, the solution is found after only one iteration.

When each particle is treated as a cluster, solving for $\boldsymbol{z}^{(k+1)}$ requires the inversion of N diagonal blocks. In the case of non-periodic flow in free space, this needs to be done only once, independent of the particle orientation: the tensorial nature of the Green's function allows us to construct the inverse of the diagonal blocks corresponding to a certain particle orientation from that for a different orientation by an orthogonal transformation. This property is especially important when multiple solutions with different relative particle positions

are to be performed as, for example, in the Monte Carlo simulation of flow through random arrays. The relative particle and particle-boundary position and orientation, however, affect the off-diagonal block elements of the master linear system; that is, they affect the matrix $\boldsymbol{N}^{\mathrm{Q}}$ on the right-hand side of (18). Treating each particle as a cluster effectively implements Faxen's law for computing the force and torque due to an incident flow used in the method of Stokesian dynamics for Stokes flow. Lubrication tractions are taken into account explicitly by means of the boundary-integral equation.

E. *Results and Discussion*

Wannier [34] derived an exact solution of the flow due to a circular particle rotating with angular velocity Ω or translating with velocity U parallel to a plane wall. His results imply that the flow can be expressed in terms of a finite sum of Stokes flow singularities located at appropriate points inside the particle and at image points with respect to the wall. The x component of the force and the z component of the torque with respect to the center of a particle, both per unit width of the particle, are given by

$$F_x = -8\pi\mu U \left(\ln \frac{y_{\mathrm{c}} + \sqrt{y_{\mathrm{c}}^2 - a^2}}{y_{\mathrm{c}} - \sqrt{y_{\mathrm{c}}^2 - a^2}} \right)^{-1} \tag{19}$$

and

$$M_z = -4\pi\mu a^2 \Omega \frac{y_{\mathrm{c}}}{\sqrt{y_{\mathrm{c}}^2 - a^2}}, \tag{20}$$

where y_{c} is the distance of the particle center from the wall and a is the particle radius. Note that as the particle approaches the wall, that is, as y_{c} tends to a from higher values, both the force and the torque tend to become singular in different functional forms. Irregular behavior of the force arises in the limit as the particle moves away from the wall due to the ill-posedness of two-dimensional infinite Stokes flow.

In Table I, we present the error in the force and torque computed using the numerical method described previously in this section, for $y_{\mathrm{c}} = 1.5a$; N_{E} is the number of boundary elements, N_{EC} is the number of collocation points per element, and N_{TC} is the total number

TABLE I

Error in the Force and Torque Exerted on a Circular Particle of Radius a Rotating with Angular Velocity Ω and Translating with Velocity U Parallel to a Plane Wall Located at $y = 0$ for $y_{\mathrm{c}} = 1.5a$

N_{E}	N_{EC}	N_{TC}	$\lvert F_x - F_x^{\mathrm{Exact}} \rvert / \mu U$	$\lvert M_z - M_z^{\mathrm{Exact}} \rvert / \mu a^2 \Omega$
8	2	16	0.01554	0.01256
16	1	16	0.01437	0.09109
8	4	32	0.00006	0.00005
16	2	32	0.00099	0.00091
32	1	32	0.00179	0.02492
8	8	64	0.00001	0.00001
16	4	64	0.00000	0.00000
32	2	64	0.00012	0.00013
64	1	64	0.00022	0.00650

of collocation points. In the boundary-integral formulation, we employ the Green's function for semi-infinite Stokes flow bounded by a plane wall, which is expressible in terms of the free-space singularity and a few singularities located at the reflection of the point force with respect to the wall [e.g., 23]. The boundary elements are native elements of a circle with equal arc lengths and are parametrized in terms of the polar angle. Using Eqs. (19) and (20), we find that the exact values for the force and torque are given by $F_x = -13.0570\ \mu U$ and $M_z = -16.8600\ \mu a^2 \Omega$.

The results in Table I illustrate the superiority of the orthogonal-collocation method over the trapezoidal discretization. For a fixed total number of collocation points, the accuracy improves dramatically as the number of element collocation points is raised while the number of elements is reduced so that their product remains constant, except for the crudest discretization with eight elements around the particle contour. For the trapezoidal discretization, increasing the number of elements by a factor of 2 reduces the error by a factor of 8, indicating a third-order discretization error. In contrast, for the spectral element discretization, increasing the number of collocation points over an element by a factor of 2 causes a seemingly exponential reduction in the numerical error. The anomalous behavior observed for $N_E = 8$ and $N_{EC} = 8$ is probably due to the accumulation of round-off error.

To perform a more demanding test, we consider a particle placed closer to the wall, $y_c = 1.05a$. In Table II, we present the error in the computed force and torque; the exact values are given by $F_x = -39.90277\ \mu U$ and $M_z = -41.21328\ \mu a^2 \Omega$. The behavior of the solution is similar to that described in the preceding paragraph. In Fig. 2, we plot the distribution of the shear stress for a particle translating parallel to the wall. The hollow circles correspond to $N_E = 64$ and $N_{EC} = 1$, and the filled squares correspond to $N_E = 8$ and $N_{EC} = 8$. It is remarkable that, for the second type of discretization, the error in the force is less than 0.05% in spite of the strong variations in the traction spanning nearly two orders of magnitude over a narrow zone of lubrication flow.

To illustrate the performance of the method for non-circular shapes, in Tables III and IV we present the force and torque exerted on an elliptical particle with major axis a and minor axis b translating parallel to a plane wall, for aspect ratio $a/b = 5$. The boundary elements are native elements of the ellipse described in terms of its natural parameter. The major or minor particle axis is perpendicular or parallel to the wall, respectively for Tables III and IV, and the clearance between the particle and the wall is $\varepsilon = 0.05a$. In the first case,

TABLE II

Error in the Force and Torque Exerted on a Circular Particle of Radius a Rotating with Angular Velocity Ω and Translating with Velocity U Parallel to a Plane Wall Located at $y = 0$, for $y_c = 1.05a$

N_E	N_{EC}	N_{TC}	$\lvert F_x - F_x^{Exact}\rvert/\mu U$	$\lvert M_z - M_z^{Exact}\rvert/\mu a^2\Omega$
8	2	16	2.19331	6.58803
16	1	16	1.47488	6.91860
8	4	32	0.21713	0.23512
16	2	32	0.62802	0.38974
32	1	32	1.41577	0.60800
8	8	64	0.01044	0.00443
16	4	64	0.01280	0.01701
32	2	64	0.18388	0.16490
64	1	64	0.37801	0.31138

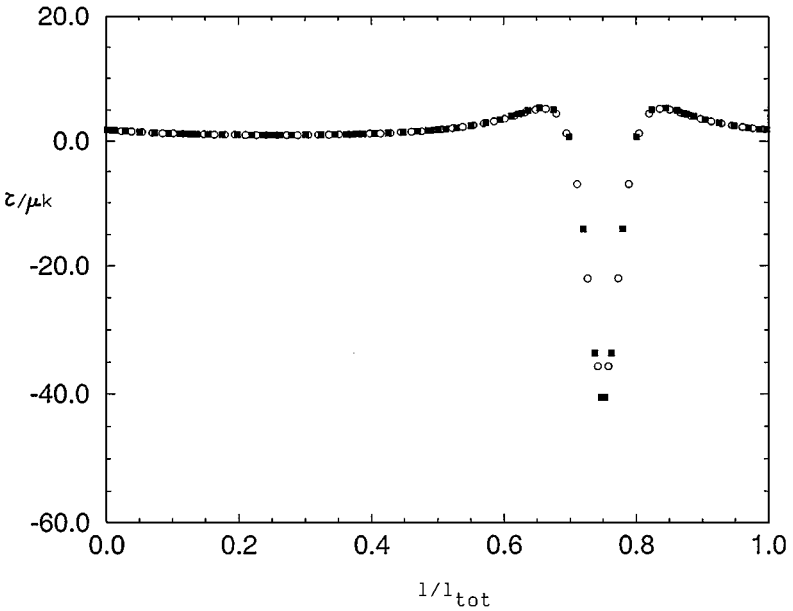

FIG. 2. Distribution of the shear stress τ over the surface of a circular particle of radius a translating parallel to a plane wall, plotted against the arc length. The center of the particle is located at a distance equal to $1.05a$ above the wall. The hollow circles correspond to $N_{\rm E} = 64$ and $N_{\rm EC} = 1$, and the filled squares correspond to $N_{\rm E} = 8$ and $N_{\rm EC} = 8$.

the results converge rapidly with increasing number of collocations, as in the case of the circular particle previously considered. In the second case, the convergence is slower due to the large extent of the lubrication zone underneath the elongated particle. In Fig. 3, we plot the distribution of the shear stress corresponding to the conditions of Table IV; the hollow circles correspond to $N_{\rm E} = 64$ and $N_{\rm EC} = 1$, and the filled squares correspond to $N_{\rm E} = 8$ and $N_{\rm EC} = 8$. In this case, the positioning of the collocation points has a strong influence on the computed distribution of the traction.

Having established the properties of the spectral-element method, we proceed to consider the issue of convergence of the iterative method expressed by Eq. (18). As a test case, we consider simple shear flow past two circular particles of radius a, separated by the distance ε, held stationary in simple shear flow. The center of the simple shear flow is placed midway

TABLE III

Force and Torque Exerted on an Elliptical Particle with Major Axis Equal to a and Aspect Ratio Equal to 5, Translating with Velocity U with the Minor Axis Parallel to a Plane Wall

$N_{\rm E}$	$N_{\rm EC}$	$N_{\rm TC}$	$F_x/\mu U$	$M_z/\mu a U$
8	4	32	−22.74495	−10.53661
16	2	32	−22.66536	−10.46246
32	1	32	−22.58783	−10.44217
8	8	64	−22.72806	−10.52162
16	4	64	−22.72825	−10.52192
32	2	64	−22.72524	−10.51882
64	1	64	−22.69395	−10.50306

Note. The clearance between the particle and the wall is $\varepsilon = 0.05a$.

TABLE IV

Force and Torque Exerted on an Elliptical Particle with Major Axis Equal to a and Aspect Ratio Equal to 5, Translating with Velocity U with the Major Axis Parallel to a Plane Wall

N_E	N_{EC}	N_{TC}	$F_x/\mu U$	$M_z/\mu aU$
8	4	32	−44.68229	73.14232
16	2	32	−44.26615	68.58008
32	1	32	−42.21933	55.01139
8	8	64	−43.82250	64.93227
16	4	64	−43.94968	66.21390
32	2	64	−43.82126	65.17173
64	1	64	−43.52646	62.91239

Note. The clearance between the particle and the wall is $\varepsilon = 0.05a$.

between the particles, so that the force exerted on the doublet vanishes preventing the logarithmic divergence of the velocity at infinity. Since the properties of the effective projection matrix associated with Eq. (18) are independent of the type of incident flow, the results are applicable to more general types of flow and orientations of the particle pair. In these test computations, each particle is treated as one cluster. In Fig. 4, we plot on a log-linear scale the root mean square of the error in the two components of the traction against the number of iterations for $\varepsilon/a = 0.20, 0.10, 0.06, 0.02$. The iterations converge at a linear rate in all cases, even in the case of nearly touching particles, but the rate of convergence is significantly reduced as the particles come closer.

Similar results were obtained for many-particle configurations, where single particles or groups of particles are treated as clusters. The rate of convergence of the iterations was found to depend on the number of clusters defined, but convergence was observed

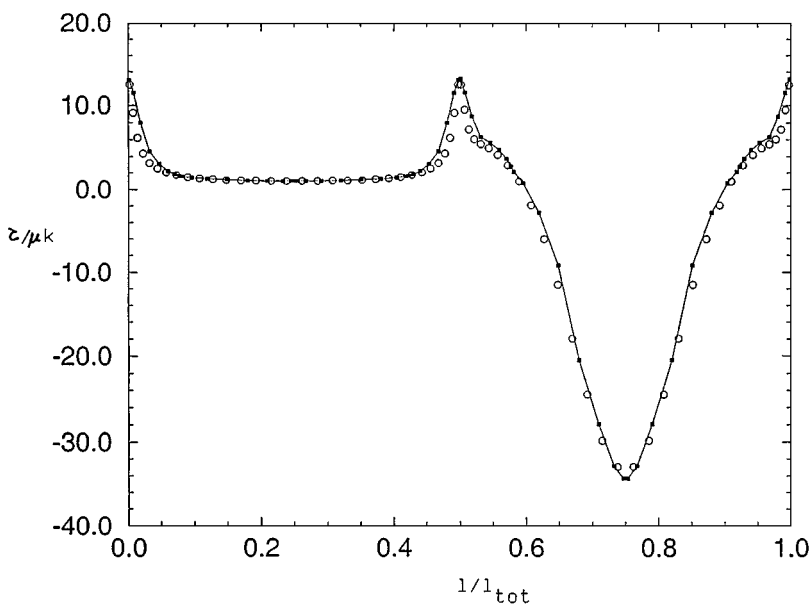

FIG. 3. Distribution of the shear stress τ over the particle surface corresponding to the conditions of Table IV, plotted against the arc length. The hollow circles correspond to $N_E = 64$ and $N_{EC} = 1$, and the filled squares correspond to $N_E = 8$ and $N_{EC} = 8$.

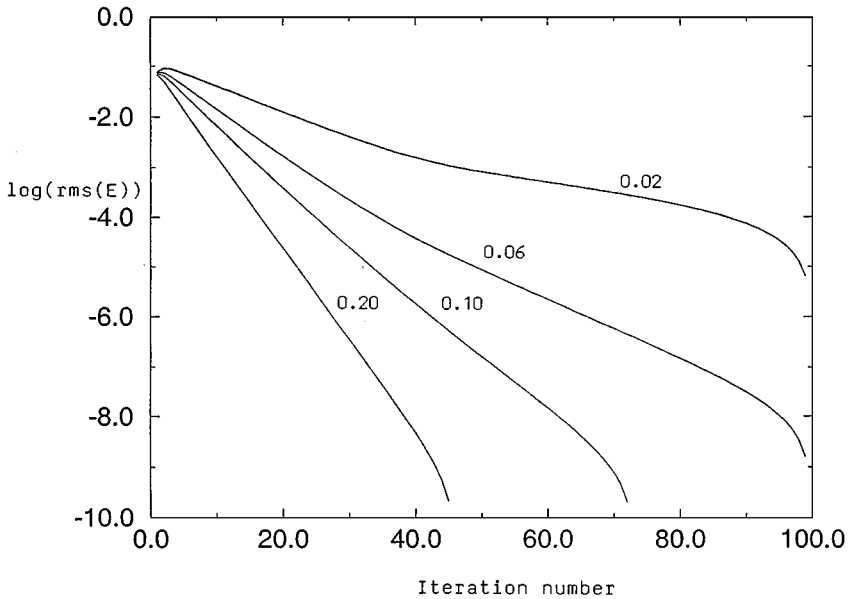

FIG. 4. Convergence test for two circular particles of radius a separated by a distance ε. Root mean square of the error in the two components of the traction plotted against the number of iterations for $\varepsilon/a = 0.20, 0.10, 0.06, 0.02$.

under demanding conditions where the particles formed agglomerates and each particle was treated as a cluster. For nearly touching particles, reducing the number of elements while holding the total number of collocation points fixed reduces the rate of convergence and under some extreme conditions may even lead to divergence.

In Fig. 5, we plot on a log-linear scale the root mean square of the error in the two components of the traction against the number of iterations for uniform flow past a random

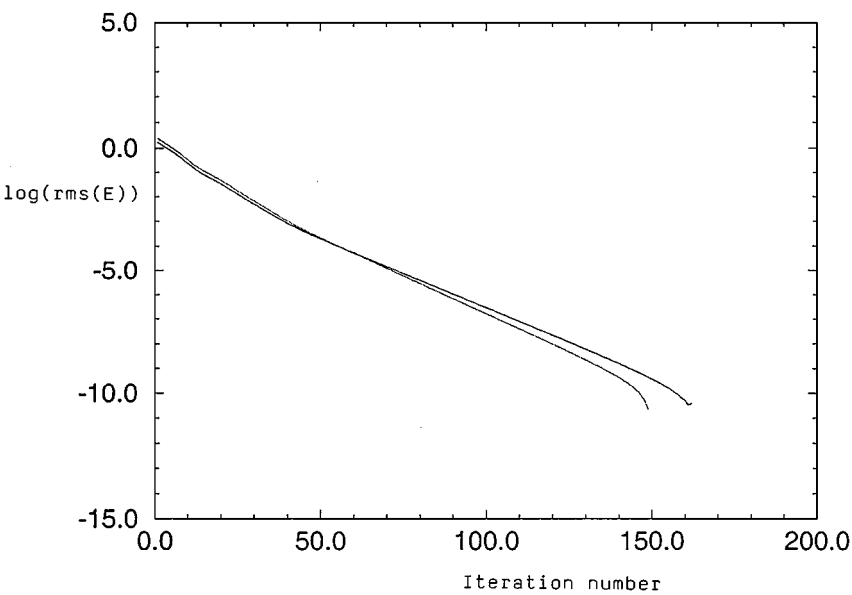

FIG. 5. Uniform flow through a doubly periodic matrix of 25 elliptical particles displayed in Fig. 6. Root mean square of the error E in the two components of the traction plotted against the number of iterations. In the iterations, each particle is treated as a cluster.

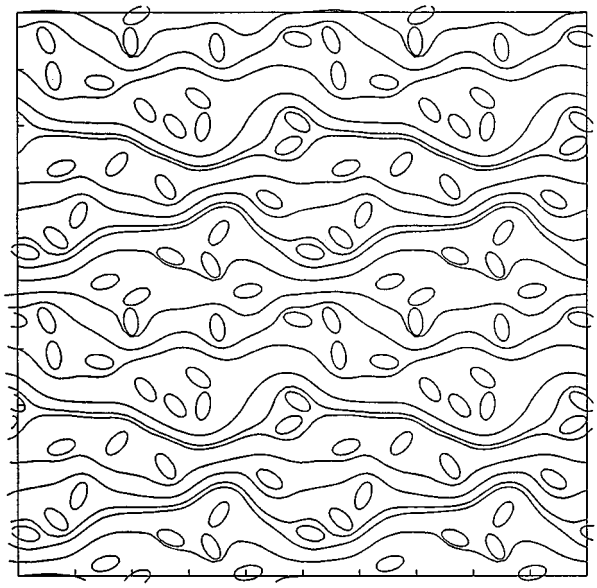

FIG. 6. Streamline pattern of uniform flow through a doubly periodic array of randomly distributed fixed elliptical particles, representing a non-consolidated porous medium.

doubly periodic lattice of 25 elliptical particles displayed in Fig. 6. The two curves correspond to two different levels of discretization with 16 or 32 elements around each particle contour, each one hosting one collocation point. In the boundary–integral formulation, we account for the periodicity of the flow by use of the doubly periodic Green's function of two-dimensional Stokes flow [28]. In this computation, each particle is treated as a cluster. Figure 5 confirms that the rate of convergence for well-separated particles is insensitive to the level of discretization. In this case, the direct solution of the master linear system would require a number of operations on the order of 10^9, whereas the inversion of the block diagonal matrices corresponding to the individual particles requires a number of operations on the order of 10^6, thus allowing for significant computational savings. The differences are exacerbated when a larger number of particles or collocation points are employed.

III. FLOW OF A SUSPENSION OF RIGID PARTICLES

In the second class of problems, we consider the flow of a suspension of rigid particles upon which a specified force or torque is exerted. In practice, the force may be due to gravity, and the torque may be due to an electromagnetic field exerted on magnetized or electrically polarized particles. The kth particle translates with velocity $\boldsymbol{U}^{(k)}$ and rotates around the z axis with respect to a designated particle center $\boldsymbol{x}_c^{(k)}$ with angular velocity $\Omega^{(k)}$, while experiencing a specified force $\boldsymbol{F}^{(k)}$ and torque $\boldsymbol{T}^{(k)}$.

To develop the boundary–integral formulation, we decompose the velocity into an incident velocity that prevails in the absence of the particles, $\boldsymbol{u}^{\infty}$, and a disturbance velocity due to the particles, $\boldsymbol{u}^{\mathrm{D}}$. Applying the boundary–integral representation at a point $\boldsymbol{x}_0$ located at the surface of the kth particle and requiring the rigid-body-motion boundary condition

$$u_j(\boldsymbol{x}_0) = U_j^{(k)} + \varepsilon_{jlm}\Omega_l^{(k)}\left(\boldsymbol{x}_0 - \boldsymbol{x}_c^{(k)}\right)_m, \tag{21}$$

we derive the integral equation

$$\frac{1}{4\pi\mu}\int_C G_{ij}(\boldsymbol{x},\boldsymbol{x}_0)\,f_i(\boldsymbol{x})\,dl(\boldsymbol{x}) + U_j^{(k)} + \varepsilon_{jlm}\Omega_l^{(k)}\big(\boldsymbol{x}_0 - \boldsymbol{x}_{\rm c}^{(k)}\big)_m = u_j^{\infty}(\boldsymbol{x}_0), \qquad (22)$$

where C is the collection of all particle contours, and $\boldsymbol{f}$ is the traction.

Specifying the force and torque exerted on the particles demands the integral constraints

$$\int_C f_i(\boldsymbol{x})\,dl(\boldsymbol{x}) = F_i^{(k)} \qquad (23)$$

and

$$\varepsilon_{zlm}\int_C f_l(\boldsymbol{x})\big(\boldsymbol{x} - \boldsymbol{x}_{\rm c}^{(k)}\big)_m\,dl(\boldsymbol{x}) = T_z^{(k)}. \qquad (24)$$

The numerical task is to solve the integro-algebraic equation (22) for the boundary traction and for the linear and angular velocities of the particle, subject to the constraints imposed by (23) and (24). As in the case of the resistance problem considered in Section II, the integral equation (22) has an infinite number of solutions; any particular solution over each particle contour may be enhanced with an arbitrary multiple of the normal vector.

To solve the integral equation (22) for the traction, we use the spectral element method described in Section II. Requiring the satisfaction of the integral equation (22) at collocation points located at the scaled zeros of Legendre polynomials over each element, and using the Gauss–Legendre quadrature to compute the integrals in (23) and (24) over each element, we find the system of linear algebraic equations $\boldsymbol{A}\boldsymbol{z} = \boldsymbol{b}$, where $\boldsymbol{A}$ is the master influence matrix, $\boldsymbol{b}$ is a constant vector, and the vector $\boldsymbol{z}$ contains the unknown values of the x and y components of the traction over all elements, as well as the particle linear and angular velocities, in the following order:

$$\begin{aligned}\boldsymbol{z} = \big(&f_x^{1,1},\, f_x^{1,2},\ldots,\, f_x^{1,N_1},\, f_y^{1,1},\, f_y^{1,2},\ldots,\, f_y^{1,N_{\rm c,1}},\, U_x^{(1)},\, U_y^{(1)},\, \Omega^{(1)}\\ &,f_x^{2,1},\, f_x^{2,2},\ldots,\, f_x^{2,N_2},\, f_y^{2,1},\, f_y^{2,2},\ldots,\, f_y^{2,N_{\rm c,2}},\, U_x^{(2)},\, U_y^{(2)},\, \Omega^{(2)}\\ &\ldots\\ &,f_x^{i,2},\, f_x^{i,2},\ldots,\, f_x^{i,N_N},\, f_y^{i,1},\, f_y^{i,2},\ldots,\, f_y^{i,N_{\rm c,i}},\, U_x^{(i)},\, U_y^{(i)},\, \Omega^{(i)}\\ &\ldots\\ &,f_x^{N,2},\, f_x^{N,2},\ldots,\, f_x^{N,N_N},\, f_y^{N,1},\, f_y^{N,2},\ldots,\, f_y^{N,N_{\rm c,N}},\, U_x^{(N)},\, U_y^{(N)},\, \Omega^{(N)}\big).\end{aligned} \qquad (25)$$

The individual scalar equations of the linear system are arranged in a similar order, with the x and y components of the force constraint (23) and the torque constraint (24) appended to the boundary–integral equations written for each particle contour. The corresponding rows of the matrix $\boldsymbol{A}$ are expressed in terms of the integration weights associated with the collocation point. Preconditioning, reduction, and iterative solution of the extended master linear system are done as discussed in Section II. The updates are based on the algorithm

$$\boldsymbol{M}^{\rm Q}\boldsymbol{z}^{(k+1)} = \boldsymbol{N}^{\rm Q}\boldsymbol{z}^{(k)} + \boldsymbol{b}^{\rm D}, \qquad (26)$$

where $\boldsymbol{M}^{\rm Q}$ is a block-diagonal matrix whose blocks correspond to particle clusters. The only new feature is that the particle velocity and rate of rotation are also updated during the iterations along with the boundary traction.

TABLE V

Velocity of Translation and Angular Velocity of Rotation of a Circular Particle of Radius a in a Symmetric Particle Pair Subjected to Simple Shear Flow with Shear Rate k

N_E	N_{EC}	N_{TC}	U_x/ka	Ω_z/k
8	4	32	0.83663	0.72173
16	2	32	0.83621	0.72217
32	1	32	0.83718	0.72112
8	8	64	0.83671	0.72165
16	4	64	0.83667	0.72169
32	2	64	0.83665	0.72172
64	1	64	0.83671	0.72165

Note. The clearance between the particle and the wall is $\varepsilon = 0.04a$.

A. *Results*

First, we illustrate the effectiveness of the spectral-element method by considering the motion of two circular force-free and torque-free particles of radius a, subject to a simple shear flow with shear rate k. The particle centers are placed perpendicular to the direction of the flow, and the clearance between the particle surfaces is $\varepsilon = 0.04a$. In the iterative solution, each particle is treated as an individual cluster of collocation points. In Table V, we present the velocity of translation and the angular velocity of rotation of one particle for an assortment of boundary elements and number of collocation points over each element. The results show that using eight elements over each particle, $N_E = 8$, and a third-order polynomial expansion, $N_{EC} = 4$, produces a velocity of translation and rate of rotation accurate to the fourth significant figure, which is adequate in dynamical simulations. Interestingly, for reasons that are not entirely clear, the accuracy of the results for 64 collocation points around each particle is insensitive to the number of elements employed.

Next, we consider the convergence of the iterative method expressed by Eq. (26). As a test case, we consider simple shear flow past two force-free and torque-free circular particles of radius a, separated by the distance ε. In Fig. 7, we plot on a log-linear scale the root mean square of the error in the two components of the traction against the number of iterations for $\varepsilon/a = 0.20, 0.10, 0.04$, corresponding to $N_E = 16$ and $N_{EC} = 2$. The iterations converge at a linear rate in all cases, but the rate of convergence is significantly reduced as the particles come closer. When $\varepsilon/a = 0.02$, the iterations diverge.

To further illustrate the performance of the method, in Fig. 8 we plot on a log-linear scale the root mean square of the error in the solution vector plotted against the number of iterations, for simple shear flow past a random doubly periodic distribution of 25 force-free and torque-free elliptical particles, corresponding to the configuration displayed in Fig. 5. The solid, dashed, and dot-dashed curves correspond, respectively, to three different levels of discretization with 16, 32, or 48 elements around each particle contour, each hosting one collocation point. In the boundary–integral formulation, we account for the periodicity of the flow by using the doubly periodic Green's function of two-dimensional Stokes flow. The iterations converge much faster than in the case of flow past a fixed array considered in Section II. This is attributed to the faster decay of the flow induced by each particle in the absence of a net force and torque exerted on it.

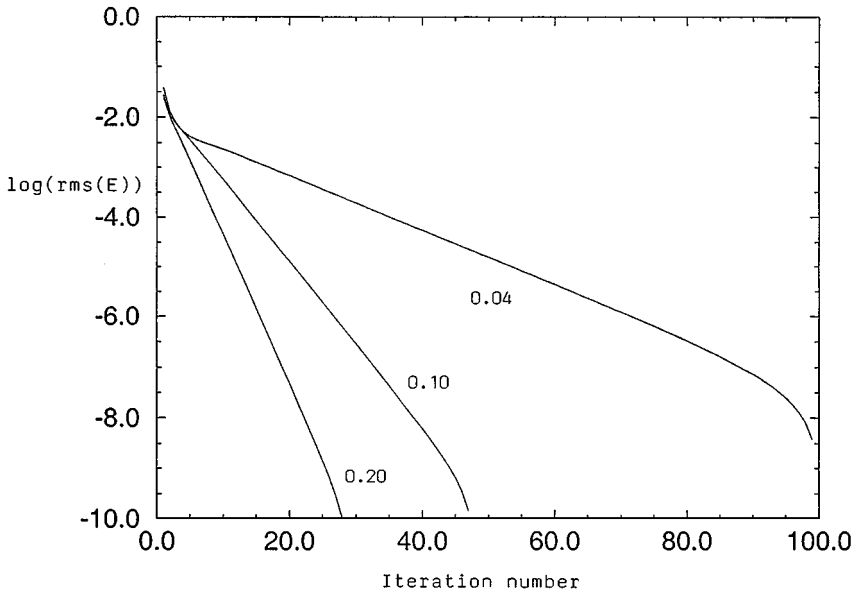

FIG. 7. Convergence test for two circular particles of radius a separated by a distance ε. Root mean square of the error E in the solution vector plotted against the number of iterations for $\varepsilon/a = 0.20, 0.10, 0.04$.

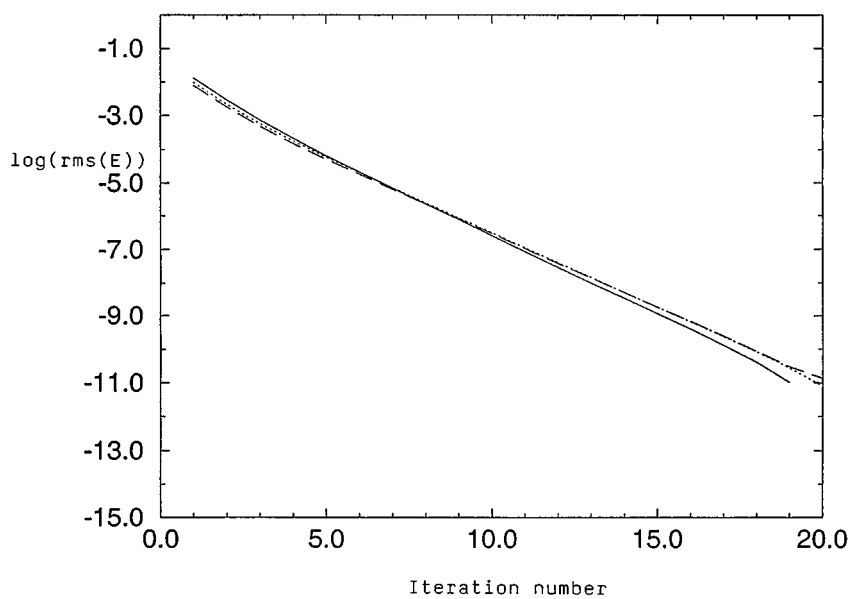

FIG. 8. Simple shear flow past a random doubly periodic distribution of 25 force-free and torque-free elliptical particles displayed in Fig. 6. Root mean square of the error E plotted against the number of iterations. In the iterations, each particle is treated as a cluster.

IV. DISCUSSION

We have made three contributions to the implementation of boundary-element methods for particulate Stokes flow. We have implemented and investigated the properties of the spectral-element collocation method building on the previous work of Higdon and co-workers [25, 26], we have developed a practical method for removing the multiplicity of solutions by projection, and we have shown that a simple iterative method for solving the master linear system converges even under demanding conditions, both for the resistance and for the mobility problem.

For the boundary-integral method to become an effective computational tool in simulating fluid–particle systems of large size, several issues must be further considered. In both the resistance and the mobility problem, the vast majority of the CPU time is expended in computing the entries of the master influence matrix by evaluating regular and singular integrals over the boundary elements. First, the computational cost may be reduced by evaluating the Green's function by means of interpolation from look-up tables [e.g., 36]. Second, when the particles are well separated, the integrand of the single-layer integral over the boundary elements shows only mild fluctuations, and this allows us to describe hydrodynamic interactions with lower resolution and to use the method of multi-pole expansions [13]. In the first approach, the rows and columns of the master influence matrix corresponding to collocation points located on well-separated particles are computed with low-order quadratures or even by trapezoidal integration. Additional simplifications might be possible by the use of the fast-summation methods for the rapid evaluation of surface integrals developed by Greenbaum and Mayo [37]. These issues are the topic of current investigation and will be discussed in a forthcoming paper along with the results of dynamical simulations.

The developments presented in this paper may be extended in a straightforward manner to three-dimensional flow. In one implementation of the boundary-element method, the surface of each three-dimensional particle is discretized into a set of triangular elements, and the three Cartesian components of the traction are expressed in terms of an expansion of basis functions developed by Dubiner [38], Sherwin and Karniadakis [39], and Heinrichs [40], involving Jacobi polynomials. Preconditioning of the master linear system and reduction may be carried out as discussed in Section II for two-dimensional flow. The integral equation is then applied at the zeros of the aforementioned basis functions or at base points of a triangle quadrature to achieve spectral accuracy. The accurate computation of the singular boundary integrals, however, requires the use of specialized quadratures for the integration of singular and weakly singular integrals over the triangles that are not available.

In conclusion, the development of accurate and efficient numerical procedures for the dynamical simulation of suspensions with a large number of arbitrarily shaped particles is a prerequisite for gaining further understandings into the dynamics of suspensions. For example, the question of whether hydrodynamic interactions between non-spherical particles yield a particle orientation distribution that is independent of the initial condition in the absence of random Brownian rotation remains unanswered [41]. If the answer is affirmative, then the probability distribution function of the particle orientation may be described by a generalized diffusion equation involving a rotational hydrodynamic diffusivity that can be evaluated from the results of dynamical simulations using methods of statistical mechanics.

ACKNOWLEDGMENT

This work was supported by the National Science Foundation.

REFERENCES

1. J. Happel and H. Brenner, *Low Reynolds Number Hydrodynamics* (Martinus–Nijhoff, Dordrecht, 1973).
2. S. Kim and S. Karrila, *Microhydrodynamics: Principles and Selected Applications* (Butterworth–Heineman, London, 1991).
3. A. Z. Zinchenko, M. A. Rother, and R. H. Davis, A novel boundary-integral algorithm for viscous interaction of deformable particles, *Phys. Fluids* **9**, 1493 (1997).
4. C. Pozrikidis, Interfacial dynamics for Stokes flow, *J. Comput. Phys.*, to appear.
5. H. A. Barnes, M. F. Edwards, and L. V. Woodcock, Applications of computer simulations to dense suspension rheology, *Chem. Eng. Sci.* **42**, 591 (1987).
6. J. F. Brady and G. Bossis, Stokesian dynamics, *Annu. Rev. Fluid Mech.* **20**, 111 (1988).
7. A. J. C. Ladd, Hydrodynamic transport coefficients of random dispersions of hard spheres, *J. Chem. Phys.* **95**, 3484 (1990).
8. J. F. Morris and J. F. Brady, Pressure-driven flow of a suspension: Buoyancy effects, *Int. J. Multiphase Flow* **24**, 105 (1998).
9. C. Chang and R. L. Powell, Dynamic simulations of bimodal suspensions of hydrodynamically interacting spherical particles, *J. Fluid Mech.* **253**, 1 (1993).
10. C. Chang and R. L. Powell, Self-diffusion of bimodal suspensions of hydrodynamically interacting spherical particles in shearing flow, *J. Fluid Mech.* **281**, 51 (1994).
11. D. I. Dratler and W. R. Schowalter, Dynamic simulation of suspensions of non-Brownian hard spheres, *J. Fluid Mech.* **325**, 53 (1996).
12. I. L. Claeys and J. F. Brady, Suspensions of prolate spheroids in Stokes flow. 1. Dynamics of a finite number of particles in an unbounded fluid, *J. Fluid Mech.* **251**, 411 (1993).
13. A. S. Sangani and G. Mo, Inclusion of lubrication forces in dynamic simulations, *Phys. Fluids* **6**, 1653 (1994).
14. G. Mo and A. S. Sangani, An O(N) algorithm for Stokes and Laplace interactions of particles, *Phys. Fluids* **8**, 1990 (1996).
15. A. J. C. Ladd, Sedimentation of homogeneous suspensions of non-Brownian spheres, *Phys. Fluids* **9**, 491 (1996).
16. H. H. Hu, Direct numerical simulation of flows of solid-liquid mixtures, *Int. J. Multiphase Flow* **22**, 335 (1996).
17. G. K. Youngren and A. Acrivos, Stokes flow past a particle of arbitrary shape: A numerical method of solution, *J. Fluid Mech.* **69**, 377 (1975).
18. T. Tran-Cong, N. Phan-Thien, and A. L. Graham, Stokes problems of multiparticle systems: Periodic arrays, *Phys. Fluids A* **2**, 666 (1990).
19. N. Phan-Thien, T. Tran-Cong, and A. L. Graham, Shear flow of periodic arrays of particle clusters, *J. Fluid Mech.* **228**, 275 (1991).
20. M. S. Ingber, Dynamic simulation of the hydrodynamic interaction among immersed particles in Stokes flow, *Int. J. Numer. Methods in Fluids* **10**, 791 (1990).
21. N. Phan-Thien and S. Kim, *Microstructures in Elastic Media; Principles and Computational Methods* (Oxford Univ. Press, New York, 1994).
22. H. Power and G. Miranda, Second kind integral equation formulation of Stokes flow past a particle of arbitrary shape, *SIAM J. Appl. Math.* **47**, 689 (1987).
23. C. Pozrikidis, *Boundary Integral and Singularity Methods for Linearized Viscous Flow* (Cambridge Univ. Press, Cambridge, UK, 1992).
24. X.-J. Fan, N. Phan-Thien, and R. Zheng, Completed double-layer boundary-element method for periodic suspensions, *Z. Angew. Math. Phys.* **49**, 167 (1998).

25. M. S. Ingber and L. A. Mondy, Direct second-kind boundary-integral formulation for Stokes flow problems, *Comput. Mech.* **11**, 11 (1993).
26. J. M. Occhialini, G. P. Muldowney, and J. J. L. Higdon, Boundary integral/spectral element approaches to the Navier-Stokes equations, *Int. J. Numer. Methods in Fluids* **15**, 1361 (1992).
27. G. P. Muldowney and J. J. L. Higdon, A spectral boundary element approach to three-dimensional Stokes flow, *J. Fluid Mech.* **298**, 167 (1995).
28. C. Pozrikidis, Computation of periodic Green's functions of Stokes flow, *J. Eng. Math.* **30**, 79 (1996).
29. G. E. Karniadakis and R. D. Henderson, Spectral element methods for incompressible flow, in *The Handbook of Fluid Dynamics*, edited by Johnson (CRC Press, Boca Raton, FL, 1998), Vol. 29-1, p. 41.
30. T. F. Chan, Deflated decomposition of solutions of nearly singular systems. *SIAM J. Numer. Anal.* **21**, 738 (1984).
31. P. C. Hansen, *Rank-Deficient and Discrete Ill-Posed Problems* (SIAM, Philadelphia, 1997).
32. K. E. Atkinson, *The Numerical Solution of Integral Equations of the First Kind* (Cambridge Univ. Press, Cambridge, UK, 1998).
33. N. Phan-Thien and D. L. Tullock, Completed double-layer boundary element method in elasticity and Stokes flow: Distributed computing through PVM, *Comput. Mech.* **14**, 370 (1994).
34. G. H. Wannier, A contribution to the hydrodynamics of lubrication, *Q. Appl. Math.* **8**, 1 (1950).
35. G. A. L. Van De Vorst, Integral formulation to simulate the viscous sintering of a two-dimensional lattice of periodic unit cells, *J. Eng. Math.* **30**, 97 (1996).
36. R. Charles and C. Pozrikidis, Effect of the dispersed phase viscosity on the simple shear flow of suspensions of liquid drops, *J. Fluid Mech.* **365**, 205 (1998).
37. A. Greenbaum and A. Mayo, Rapid parallel evaluation of integrals in potential theory on general three-dimensional regions, *J. Comput. Phys.* **145**, 731 (1998).
38. M. Dubiner, Spectral methods on triangles and other domains, *J. Sci. Comput.* **6**, 345 (1991).
39. S. J. Sherwin and G. E. Karniadakis, A triangular spectral element method—Applications to the incompressible Navier-Stokes equations, *Comput. Methods Appl. Mech. Eng.* **123**, 189 (1995).
40. W. Heinrichs, Spectral collocation on triangular elements, *J. Comput. Phys.* **145**, 743 (1998).
41. G. K. Batchelor, Transport properties of two-phase materials with random structure, *Annu. Rev. Fluid Mech.* **6**, 227 (1974).